SANDIA REPORT

SAND2007-8000
Unlimited Release
Printed March 2008

Characterization of Shape Memory Alloys for Safety Mechanisms

Jordan E. Massad, Thomas E. Buchheit, and Jared T. McLaughlin

Prepared by
Sandia National Laboratories
Albuquerque, New Mexico 87185 and Livermore, California 94550

Sandia is a multiprogram laboratory operated by Sandia Corporation,
a Lockheed Martin Company, for the United States Department of Energy's
National Nuclear Security Administration under Contract DE-AC04-94AL85000.

Issued by Sandia National Laboratories, operated for the United States Department of Energy by Sandia Corporation.

Available to DOE and DOE contractors from
U.S. Department of Energy
Office of Scientific and Technical Information
P.O. Box 62
Oak Ridge, TN 37831

Telephone: (865) 576-8401
Facsimile: (865) 576-5728
E-Mail: reports@adonis.osti.gov
Online ordering: http://www.osti.gov/bridge

Available to the public from
U.S. Department of Commerce
National Technical Information Service
5285 Port Royal Rd.
Springfield, VA 22161

Telephone: (800) 553-6847
Facsimile: (703) 605-6900
E-Mail: orders@ntis.fedworld.gov
Online order: http://www.ntis.gov/help/ordermethods.asp?loc=7-4-0#online

SAND2007-8000
Unlimited Release
Printed March 2008

Characterization of Shape Memory Alloys for Safety Mechanisms

Jordan E. Massad
Applied Mechanics Development

Thomas E. Buchheit
Microsystem Materials

Jared T. McLaughlin
Integrated Surety Mechanisms I

Sandia National Laboratories
PO Box 5800
Albuquerque, New Mexico 87185-1070

Abstract

Shape memory alloys (SMAs) are metals that exhibit large recoverable strains and exert large forces with tremendous energy densities. The behavior of SMAs is thermomechanically coupled. Their response to temperature is sensitive to their loading condition and their response to loading is sensitive to their thermal condition. This coupled behavior is not to be circumvented, but to be confronted and understood, since it is what manifests SMA's superior clamping performance. To reasonably characterize the coupled behavior of SMA clamping rings used in safety mechanisms, we conduct a series of experiments on SMA samples. The results of the tests will allow increased fidelity in modeling and failure analysis of parts.

Acknowledgments

The authors greatly appreciate the guidance, resources, and assistance provided by the following staff members: Michael Hosking, Saundra L. Monroe, Matthew A. Neidigk, David T. Schmale, Donald Susan, and Rajan Tandon. In particular we acknowledge Denise N. Bencoe and Thomas B. Crenshaw for their acquisition of the experimental data discussed in this report. We also appreciate Thomas Borden (Intrinsic Devices, Inc.) for his guidance in using his testing materials.

Table of Contents

Figures

Tables

Nomenclature

FE	Finite element.
M_d	High temperature limit for stress-induced transformations, [°C]
RT	Room temperature, [°C]
SMA	Shape memory alloy.

1. Introduction

Shape memory alloys (SMAs) are metals that exhibit large recoverable strains (up to 10%) and exert large forces with tremendous energy densities. SMAs undergo martensitic transformations, which are displacive transformations dominated by shear distortions of the crystal lattice. Transformations occur between solid phases and are referred to as the martensite and austenite phases. Distinguished by their crystallographic structures, martensite and austenite can have drastically different mechanical, thermal, electrical, optical, and acoustical material properties [9]. In general, martensite is the material phase that is stable at low temperatures relative to austenite, which is stable at high temperatures.

1.1. Nonlinear Thermomechanical Behavior

The martensitic transformations between martensite and austenite enable SMAs to recover or "remember" shape by two different mechanisms. In both cases, austenite corresponds to the remembered shape. First, superelasticity describes shape memory via stress-induced phase transformations. At a fixed temperature where stress-free austenite is a stable phase, austenite transforms into martensite due to an applied load. Upon removing the load, the material reverts to austenite and the original shape is recovered. Secondly, the shape memory effect describes shape memory via temperature-induced transformations. In this case, deformed martensite transforms into austenite due to heating and shape memory is observed. Upon subsequent cooling, the SMA transforms back to martensite. If the SMA is stress-free upon cooling, then it will retain its recovered shape in the martensite phase by means of a process called self-accommodation. If the SMA is subjected to a load while cooling, then it will deform again as it reverts to martensite.

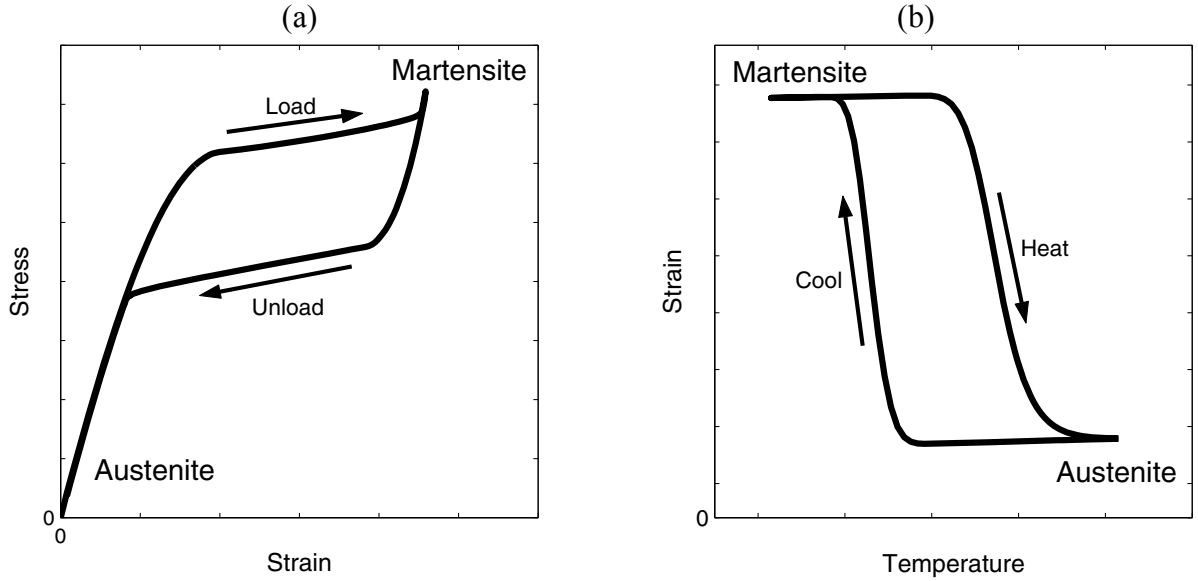

Figure 1.1: Nonlinear thermomechanical response of SMAs: (a) superelasticity and (b) shape memory effect.

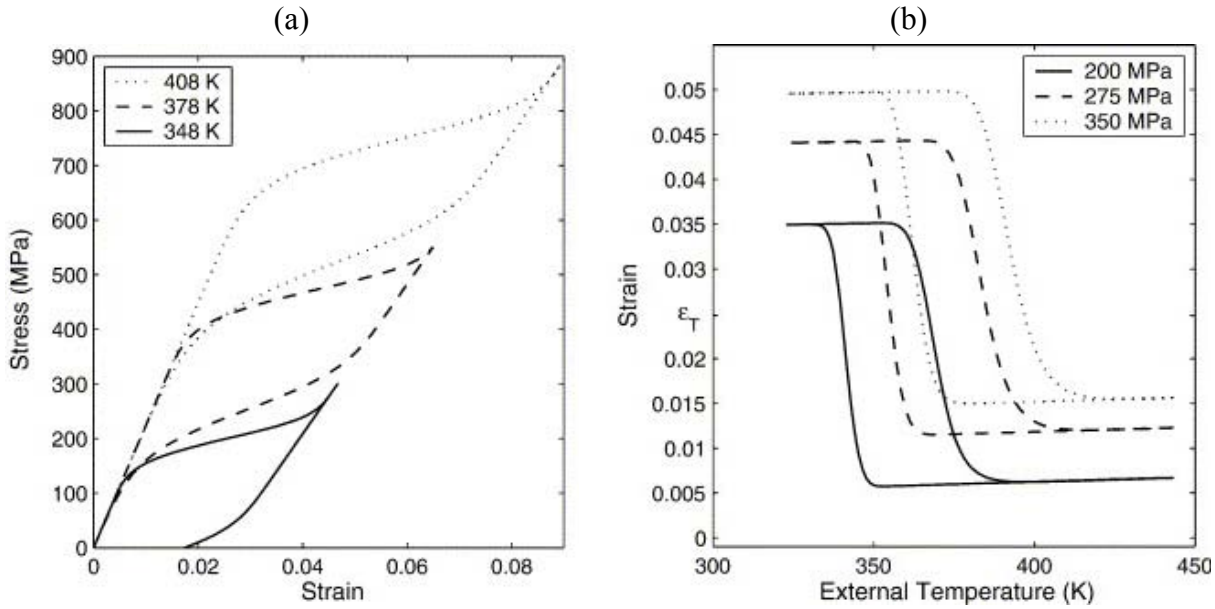

Figure 1.2: Thermomechanically coupled behavior of SMAs: (a) temperature dependence of the stress-strain response, and (b) stress dependence of the temperature-strain response.

As illustrated in Figure 1.1, hysteresis is associated with both superelasticity and the shape memory effect. For superelasticity, it is observed that austenite deforms elastically until a loading transformation is reached. Further loading induces a transformation to the martensite phase with a large transformation strain. Upon unloading martensite, the transformation strain is recovered as the SMA returns to austenite. For the shape memory effect, hysteresis is often observed when an SMA is subjected to a fixed load. In this case, an austenitic SMA will transform to martensite when cooled, exhibiting a large transformation strain in the process. When reheated to austenite, the transformation strain is recovered.

The general stress–temperature–strain behavior of SMAs is thermomechanically coupled, as illustrated in Figure 1.2. Figure 1.2a shows that the stress–strain response depends on the state of temperature. Typically, as the temperature increases, the transformation stress increases and the hysteresis loop shifts upward accordingly. Figure 1.2b shows that the temperature–strain response depends on the state of stress. As the stress increases, the transformation temperature increases.

There are many different compositions of SMA. NiTi is the most fabricated, studied, and used SMA. Ternary alloys based on NiTi have been developed to achieve certain material properties. For example, NiTiNb with 6% to 20% (atomic) Nb content has been fabricated to provide a fairly wide thermal hysteresis [1,4]. The thermal hysteresis of NiTiNb has been shown to be as wide as 150 °C, that is, there is a 150 °C difference between the heating temperature at which the SMA transforms to austenite and the cooling temperature at which it reverts to martensite. The addition of Nb to NiTi provides a microstructure consisting of predominantly a dispersion of Nb particles in a NiTi matrix [9,13]. Ultimately, in addition to widening the thermal hysteresis when compared to NiTi, the Nb particles add plastic, irreversible strains to the ideal shape memory deformations illustrated in Figures 1.1 and 1.2**.** NiTiNb is the focus of this paper and the reader is referred to [9] for details of shape memory mechanisms, SMA material properties, and other alloy compositions.

1.2 SMA-based Safing Wheel Design

The hysteresis exhibited by shape memory alloys enables the materials to achieve very high work densities, produce large recoverable deformations, and generate high stresses, which are ideal for high performance applications. For example, SMAs have been considered for medical and potential aeronautic and aerospace applications that require large deformations and large forces [9]. In particular, owing to its typically wide hysteresis, NiTiNb SMAs have been studied for medical, mechanical damping, and coupling device applications [1, 3, 14, 16, 18]. Figure 1.3 illustrates the clamping ring concept, where a pre-dilated martensite SMA ring reverts to a smaller diameter shape corresponding to its remembered shape in the austenite phase. The wide hysteresis of NiTiNb is ideal for permanent clamping rings, since, after heating to an elevated austenite transformation temperature (e.g., 60 °C), the rings remain austenitic and retain their clamping force even upon subsequent cooling to temperatures experienced during further assembly and component operation. Due to the wide thermal hysteresis, relaxation of the ring does not occur until relatively low, subambient temperatures are reached (e.g., -90 °C). The size and position of the transformation hysteresis can be tailored via changes in alloy composition and material processing [1, 14, 20].

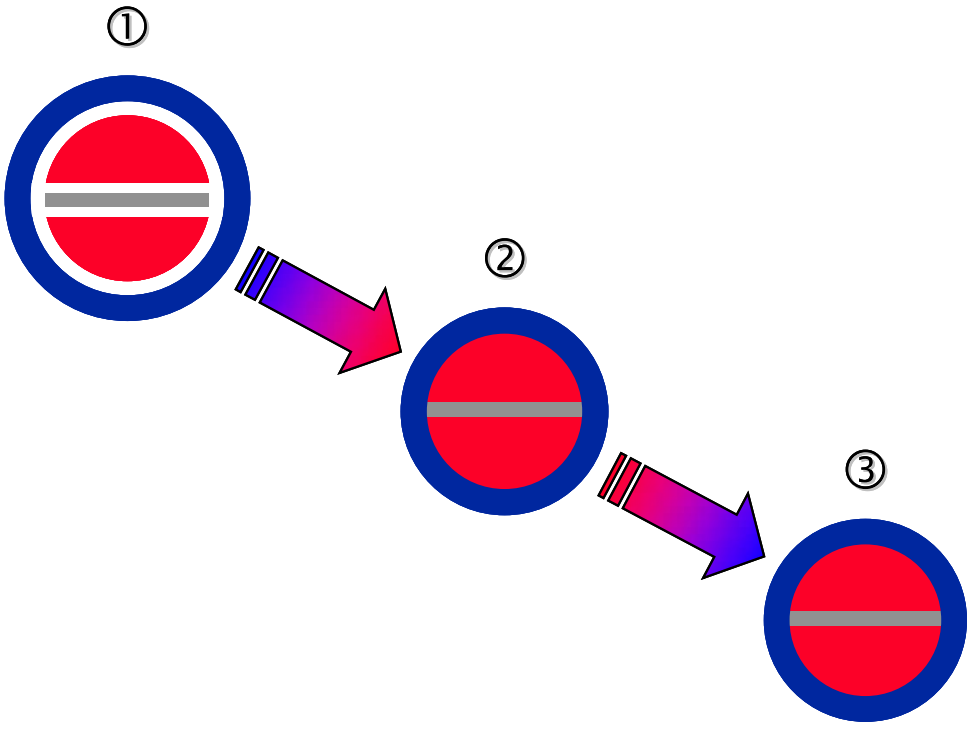

Figure 1.3: SMA Clamping Ring Concept: (1) martensite SMA ring is placed around an assembly, (2) ring is heated to austenite and shrinks, thereby clamping the assembly, and (3) the clamping force remains as the ring cools to ambient temperature austenite.

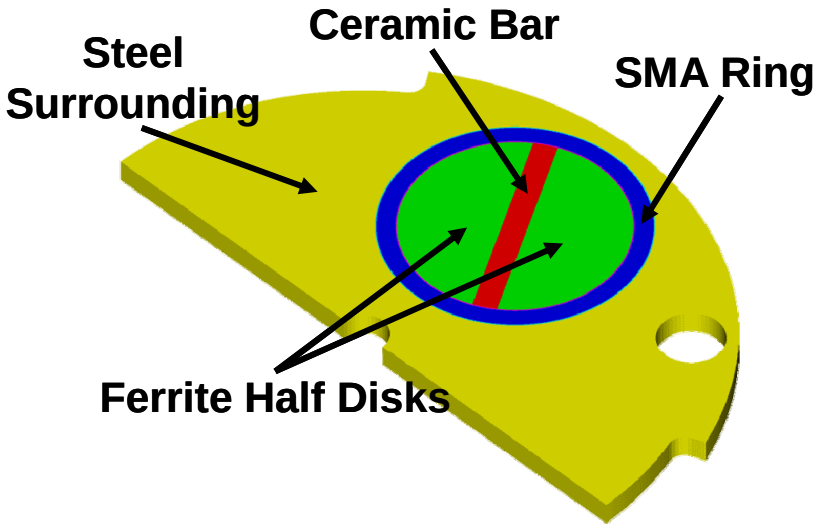

Figure 1.4: SMA-based design of safing wheel.

In this report, we discuss the characterization of NiTiNb used in clamping rings. The material, termed Alloy-H, is manufactured by Intrinsic Devices, Inc. and has the composition Ti 45%, Ni 46.4%, Nb 8.6% (atomic percent). The millimeter-size rings are used in the shutter portion (called the "safing wheel") of an interrupted transformer safety switch. Half of the safing wheel design is illustrated in Figure 1.4, where within a steel surrounding, an SMA ring surrounds two ferrite half-disks and a ceramic bar. During installation, the rings shrink considerably and forcibly to clamp the ferrite half-disks with the ceramic bar. Previous designs of the safing wheel have metallized the outside diameter of the ferrite disks and then soldered the disks to a non-magnetic ring such as copper. Mechanical integrity of the metallized/soldered joints has always been marginal due to the relatively very weak and brittle ferrite and controlling the process to ensure consistent adhesion of the metal layers extremely difficult. This SMA-based design greatly simplifies the assembly process and obviates the very process-sensitive metallization/solder method while preloading the ceramics in compression, making the assembly very robust to mechanical environments.

Unfortunately, the loading of the ferrite/ceramic sub-assembly by the shrinking SMA ring does not result purely in radial compression. It was discovered early in development of the design that tension great enough to cause fracture can be imparted on the ferrites depending on the size of the ring selected, the fixturing during shrinking, the surface condition of the ferrite, etc. Therefore it became necessary to understand the mechanisms causing the tension so that the design and/or the assembly process could be modified to mitigate the stress. To reasonably characterize the coupled behavior of SMA clamping rings, we conducted a series of experiments on NiTiNb Alloy-H samples. The results of the tests allow increased fidelity in modeling and failure analysis of the parts. In Section 2, we discuss the non-loaded temperature-strain response and transformation temperatures. In Section 3, we summarize the stress-temperature, stress-strain, and stress-strain-temperature response. In Section 4, identification of model parameters from the measured data is discussed. Finally, concluding remarks are included in Section 5.

2. Dilatometry and Differential Scanning Calorimetry

Initially, as-received SMA rings (AHE0557-0046-0085) used in the safing wheel design were measured and then heated to 150 °C in an oven. After the rings cooled to room temperature (RT), new measurements showed that the inner diameter had contracted an average of 6.1%, while the axial length had expanded an average of 2.3%. To assess the impact the shape changes have on the ferrite core during assembly, it was necessary to investigate how the rings evolve from their initial state to their final state. The investigation began with stress-free thermal measurements at Sandia's Advanced Materials Laboratory. These measurements included dilatometry to assess thermal strains and differential scanning calorimetry (DSC) to identify transformation temperatures. In addition to clamping rings, the Alloy-H thermal test samples included cylindrical rods (PHE0125-0250) that shrink axially when heated, in the same manner that the clamping rings contract radially.

2.1 Dilatometry

Thermal strain was measured independently in the radial and axial directions. Nominally, the cylindrical rods had a length and diameter of 0.250 inch and 0.125 inch respectively. Figure 2.1 plots the measured contraction of the rods while heated at a rate of 2 °C/min up to 310 °C, then cooled at the same temperature rate to 22 °C. For each case, the strain is relative to the length measured in the apparatus at the beginning of the heating cycle.

Rods 1 and 2 were heated from 22 °C. Contraction was observed beginning at around 30 °C, indicating the start of the martensite-austenite transformation; 90% of the total contraction occurred at 60 °C and 99.9% occurred up to 210 °C. At temperatures greater than 210 °C, linear thermal expansion is observed, indicating that the sample is almost completely austenite. Upon cooling, the austenite rods contract due to linear thermal contraction. Linear behavior was observed for subsequent heating and cooling cycles.

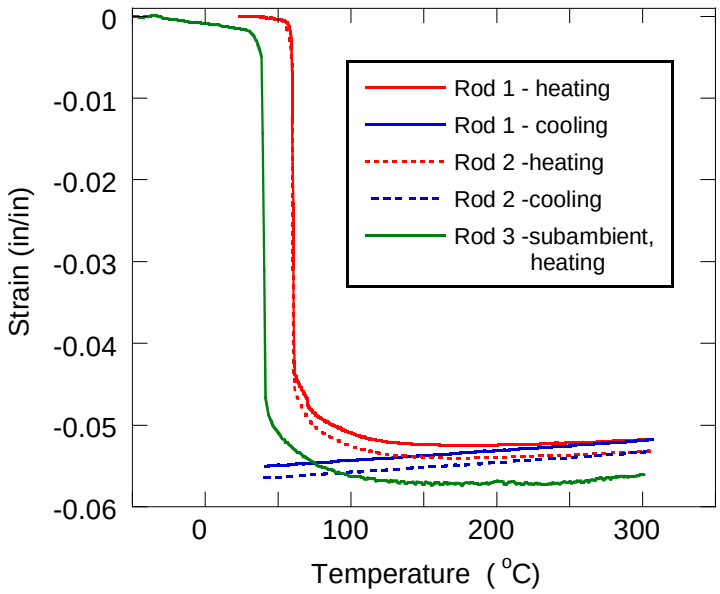

Figure 2.1: Dilatometry of rods quantifies the radial contraction of the SMA rings.

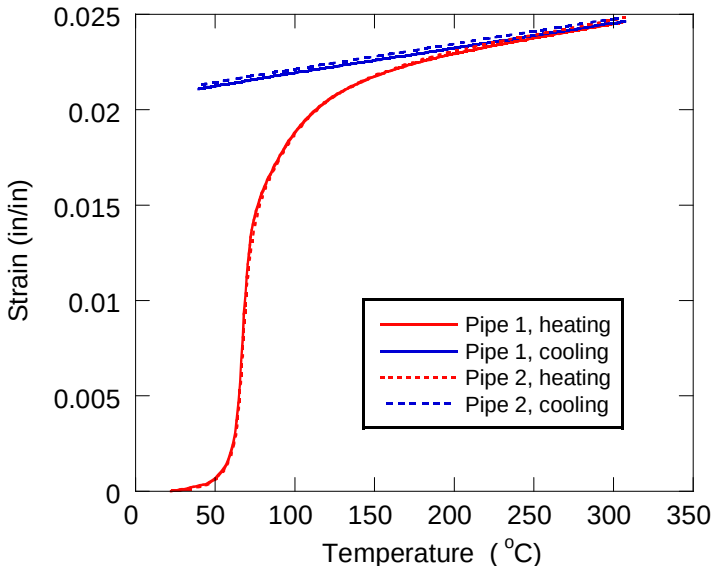

Figure 2.2: Dilatometry of pipes quantifies the axial expansion of the SMA rings.

Rod 3 was cooled with liquid nitrogen to −50 °C and subsequently heated at 2 °C/min in a thermomechanical analyzer. The rod contracted negligibly during the cooling to −50 °C, but the pre-treatment resulted in a lowering of the transformation temperature to 40 °C, which indicates the sensitivity of the NiTiNb behavior to processing and its initial condition [1, 2, 4, 6, 12, 20]. The effect of cooling NiTiNb on its heating transformation behavior has not been studied; therefore more testing is required to better understand this observed phenomenon. Ultimately, however, pre-cooling is not performed in part delivery or installation for the safing wheel. Comparing the initial diameters to the diameters after testing, those of each rod increased by approximately 2.6%.

The axial lengths of the clamping rings to be used in the safing wheel are too short for the dilatometer to accurately measure the differential axial displacement imparted by the martensitic transformation. Therefore, to measure the thermal response in the axial direction of the rings, Alloy-H rings with long axial lengths, termed *pipes*, were obtained (AHE0188-0039-0262). As-received, the axial length and outer diameter were 0.265 in and 0.268 in, respectively. Figure 2.2 plots the measured elongation strain of the pipes as they shrink in diameter while heated at a rate of 2 °C/min up to 310 °C, followed by cooling to 22 °C. Comparing the initial outer diameters to the outer diameters after testing, those of each pipe decreased by approximately 3.6%.

Analogous to the contraction of the rods, axial expansion of the pipes was observed to begin near 30°C, indicating the start of the martensite-to-austenite transformation. However, the expansion did not occur as abruptly, and only about 60% of the total expansion had occurred by 70°C. At temperatures greater than 210°C, linear thermal expansion is observed, indicating that the sample is almost completely austenite. Figure 2.2 shows that upon cooling, similar to the behavior of the rods, the austenite pipes contract only due to linear thermal contraction. Linear behavior was observed for subsequent heating and cooling cycles.

The fact that the rings grow axially as they shrink radially is significant. Using the data presented here, this non-isotropic behavior is incorporated into simulations of the SMA-based safing wheel assembly in [15].

2.2 Differential Scanning Calorimetry

DSC provides an independent measurement of the thermal transformation behavior of the SMA rings. In the last 25 years, DSC has been the primary method for determining transformation temperatures and heat capacities of SMAs [9, 17]. DSC hinges upon the fact that phase transformations are exothermic or endothermic reactions. As an SMA is heated or cooled, DSC monitors an increase or decrease in heat flux, thereby indicating when a transformation takes place.

Two Alloy-H rings (AHE0110-0033-0033) were measured via DSC. Figure 2.3a plots the results for a ring heated from RT and Figure 2.3b plots the results for a ring heated from 2 °C, which was cooled prior to testing. In both plots, the peak in heat flow corresponds to the transformation from martensite in the as-received condition to austenite. The temperatures noted on the plots represent transformation indicators. The transformation starts at approximately 40 °C and ends at approximately 120 °C in load-free conditions. These results agree with the dilatometry results in Section 2.1, where upon heating, contraction was observed from 40-140 °C. The effect of cooling the SMA prior to testing may be responsible for the slight decrease in DSC peak temperature from 68.2 °C to 60.1 °C. This observation corroborates the decrease in transformation temperature observed in Figure 2.1 where the SMA was cooled to even lower temperatures. In the next section, the response of NiTiNb Alloy-H under both changing temperature and loading is discussed.

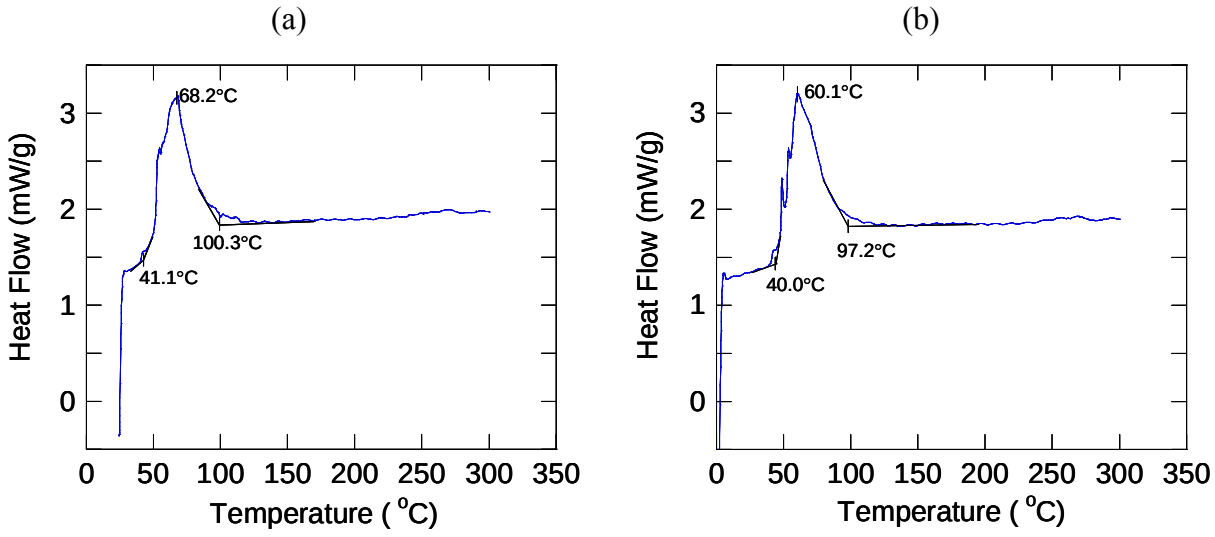

Figure 2.3: DSC of Alloy-H rings heated to 300 °C from (a) 24 °C (b) and 2 °C.

This Page intentionally left blank

3. Thermomechanical Tension Experiments

The experiments described in the previous section are necessary for understanding how the SMA rings react to heating under zero loading. This section presents results from measurements of the coupled thermomechanical response. Similar experiments have been conducted on other various compositions of NiTiNb in [1, 5, 8, 10, 19]. Alloy-H tension rods were provided and processed by Intrinsic Devices so that they shrink axially in the same manner that the rings contract radially, similar to the rods measured with dilatometry in Section 2.1. Figure 3.1 shows the manufacturer's schematic of the tension rods.

The rods were tested in a standard MTS servohydraulic load frame equipped with a convection oven style thermal chamber. Testing was controlled using a Test Star IIs system permitting switches from load control to strain control necessary for several of the experiments. Strain measurements were performed using contact extensometery and non-contact laser extensometry. Contact extensometry was typically performed with a MTS model 632 12C-20 contact extensometer, providing a strain resolution of approximately 0.05% across a 1 inch gage length rated for use up to 130 °C. Non-contacting laser extensometry was performed using an Electronic Instruments Research model LE-01 laser extensometer, which had a displacement resolution of 0.001 in. Strain rates were kept to approximately 10^{-4}/s to avoid material self-heating and heating rates were kept at or below 2 °C/min. Rate-dependent material self-heating of SMAs during tension tests is discussed in [8, 11].

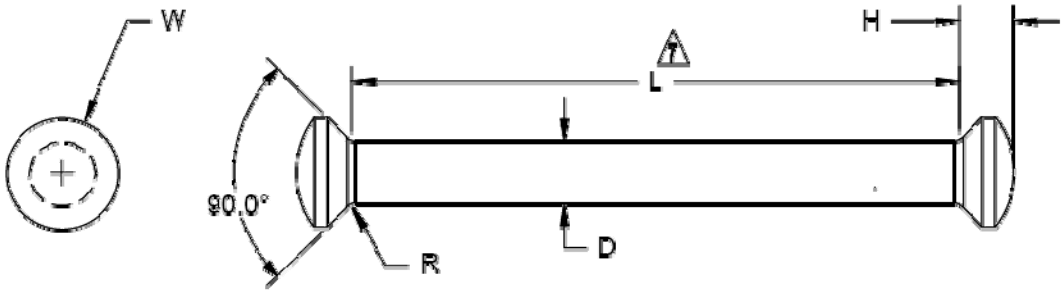

Product Description	L Minimum Supplied	L Maximum Recovered	D Supplied	H Maximum Supplied	W Maximum Supplied	R Maximum Supplied	Minimum Constraint Length	Nominal Tensile Force (lbs)
THE6000-0125	6.000	5.720	0.125±.002	.140	0.240	0.030	5.806	370

Figure 3.1: NiTiNb tensile rod specification supplied by Intrinsic Devices, Inc.; length units are inches.

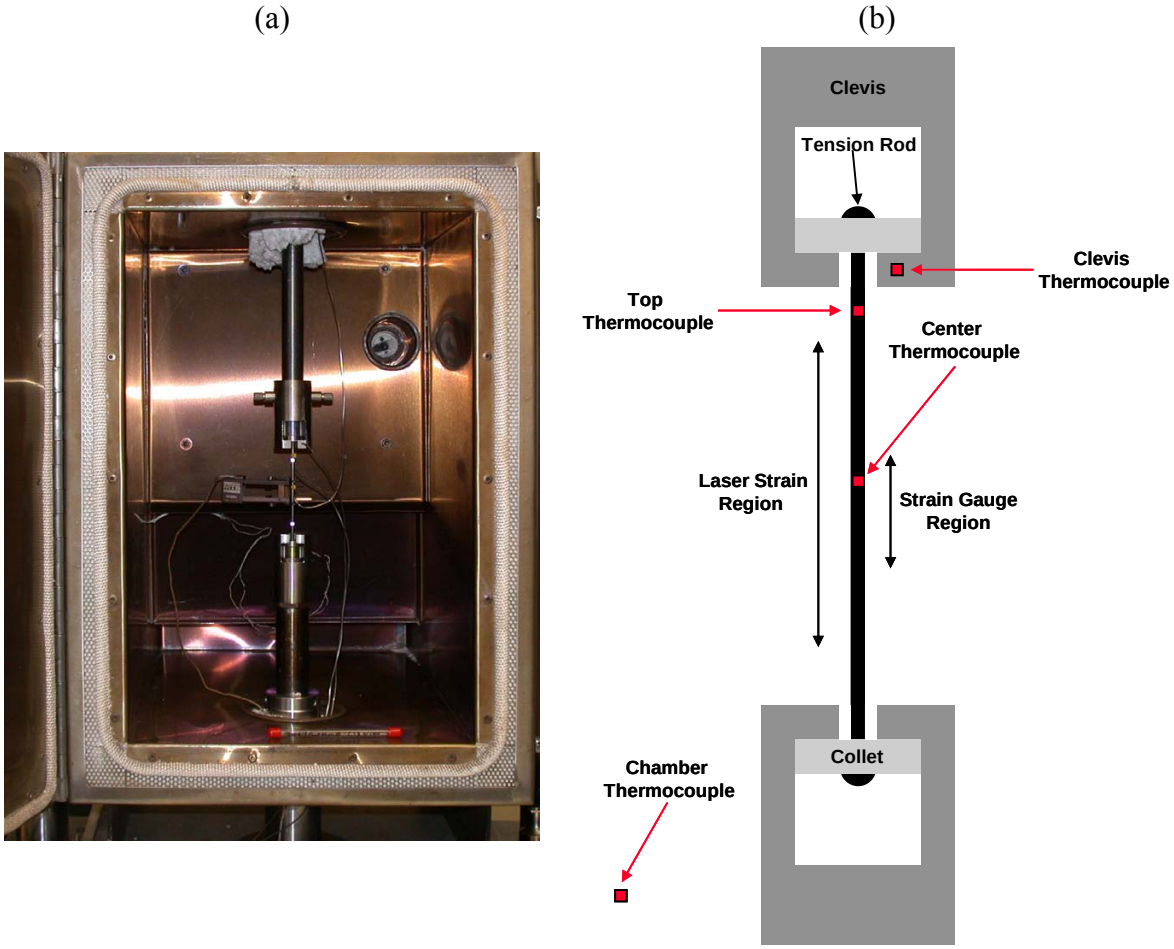

Figure 3.2: Tensile test setup in thermal chamber: (a) photo and (b) diagram.

A wide range of experiments were conducted: null-load thermal strain experiments; temperature-controlled tension tests; temperature controlled strain and stress experiments, and tension tests of partially transformed rods. Appendix A tabulates details of each test performed and the results are summarized here. A figure of the experimental set-up, with a tensile rod in position for testing is given in Figure 3.2. Figure 3.2a is a photo of a typical set-up and Figure 3.2b is a corresponding schematic diagram. Figure 3.2b illustrates two gage sections, indicating the simultaneous strain measurement of the contact extensometer and non-contact laser extensometer. The contact extensometer measurements were used to govern all but one of the strain control experiments. The non-contact laser measurements relied on position changes of reflective tape placed at specific locations on the tensile rods. The initial spacing of the reflective tape, which represented the initial gage length for this measurement, was 1.0 in, 2.0 in, or 3.0 in. In addition, the tape was offset from the contact extensometer position. The primary goal of the non-contact strain measurement was to provide an additional, independent, and comparative measure of strain in the thin section of the tensile rods. The temperature in the chamber was manually controlled and monitored primarily by a thermocouple mounted near the center of the test specimen, as indicated in Figure 3.2b.

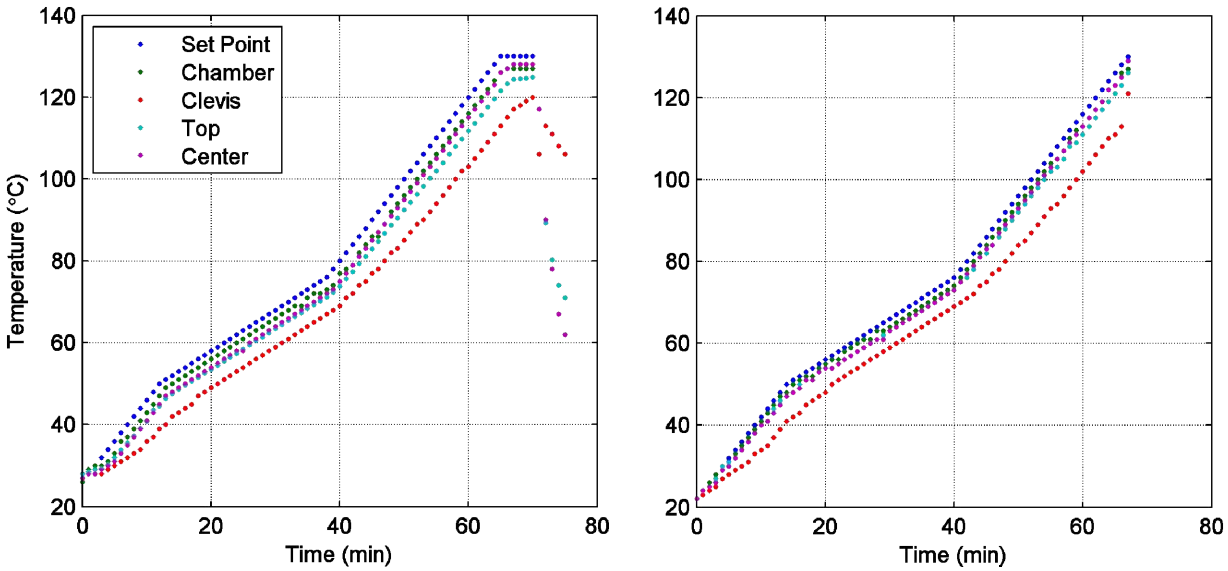

Figure 3.3: Evolution of temperature distribution along tension rods and in the chamber from two experiments.

To identify potential thermal gradients in the specimen, temperature was monitored at additional locations indicated in Figure 3.2b. Figure 3.3 plots the temperature measurements at these locations from two experiments. The results of the two tests are similar across the temperature range of interest, indicating that the temperature gradients within the chamber were consistent across all the experiments. The chamber temperature was monitored by the chamber thermocouple; it was typically higher than the temperature measured at the center thermocouple by approximately 3-5 °C, even with a heating rate as low as 1 °C/min. In addition, temperature monitoring at the clevis, the fixturing used to secure the test sample, indicated a temperature differential of up to 6 °C between the clevis and the test sample. However, the average temperature difference from the center to the top position of the rod was less than 2 °C. These results indicate that the thermal mass of the clevis most likely provided a conductive heat sink. Although there was a small gradient across the thin section of the tensile rods, it was typically in an acceptable range of 1-2 °C.

3.1 Null-load Thermal Strain Experiments

To evaluate the baseline thermal response of the SMA rods within the tension test configuration, a series of three "null-load" thermal strain tests were conducted. For each of these tests, a small tensile load of approximately 5 lbf (0.4 ksi) was applied to hold the SMA tensile rod securely in place and the temperature was increased to a final temperature of either 125 °C or 140 °C. The small load was expected to have a negligible effect on the temperature-strain response of the SMA rod. Strain was monitored throughout the experiments and the resulting strain-temperature curves from all three experiments are given in Figure 3.4. The results were similar to those reported in Section 2.1 from the Alloy-H cylindrical rods. The bulk of the transformation-strain occurred near 60 °C and the total contraction due to the martensite-to-austenite transformation was about 5.7%. The nearly identical strain-temperature response between the Alloy-H specimens used for the dilatometry experiments and the Alloy-H tensile rods indicate that the

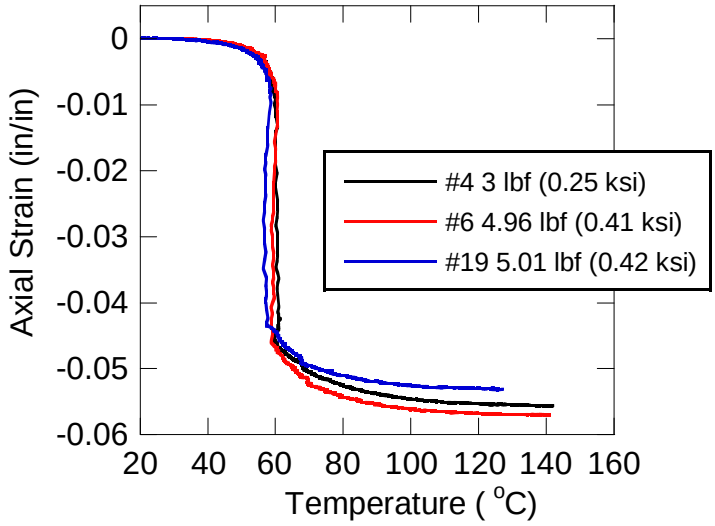

Figure 3.4: Strain vs. Temperature curves from three null-load experiments performed on Alloy-H tensile rods.

tensile rods have shape-memory characteristics that are indistinguishable to the cylindrical dilatometry specimens. Furthermore, the rods used for tensile testing and the specimens used for dilatometry measurements were fabricated from a different lot of material, suggesting that the supplier is able to produce the NiTiNb alloy with minimal lot-to-lot variation.

3.2 Temperature Controlled Tension Test Experiments

Three series of tension test experiments were performed with the intent of mapping the stress-strain response across a range of temperatures encompassing the martensite-to-austenite transformation. The first series characterizes the RT response of the Alloy-H SMA in its as-received martensitic state and its fully transformed austenitic state. The second series characterizes the stress-strain response of Alloy-H during several intermediate thermal excursions between RT and 140 °C. The test temperature dictates whether and how much of the material has transformed to austenite. These experiments were primarily conducted at temperatures above 60 °C, thus a majority of the material within the gage section of the test specimens had transformed to austenite prior to tensile testing, per results given in Section 2 and Figure 3.4. The third series of experiments characterized the stress-strain response of the transformed material on cooling to several temperatures after a 140 °C excursion. In this series, the rods were expected to be fully austenitic prior to tensile testing.

The series of tensile stress-strain curves generated from RT experiments of as-received Alloy-H specimens is given in Figure 3.5. Figure 3.5a shows a plot of the entire stress-strain curves from four experiments. An unload/reload excursion was also performed in one experiment after 3% strain; that result is included in Figure 3.5a and separately in Figure 3.5b. The hysteretic response observed in the unload/reload excursion is attributed to a nonlinear, semi-reversible microstructure deformation phenomena in martensitic SMAs referred to as *martensitic detwinning* [5, 9]. Figure 3.5b also shows comparative stress-strain curves generated simultaneously from the default extensometer, the laser extensometer, and a high resolution extensometer (MTS model 632 27C-20). The high resolution extensometer provided a strain

resolution of about 0.015% and was limited to 4% strains and only moderate testing temperatures. The laser extensometer measured displacement across a 2 in gage section for this test. The inferior resolution of the laser extensometer can be observed by the comparative scatter shown in Figure 3.5b. Ultimately, the comparison of stress-strain results between all three strain measurements was favorable.

Figure 3.6 shows RT tension test results of two Alloy-H specimens after a 30 min soak at 140 °C prior to testing. These samples were assumed to have fully transformed to the austenite phase due to this elevated temperature excursion. Test 25 was a non-cyclic tension test and Test 30 included three successive unload/reload cycles to zero stress. The overall stress-strain response from both tests was similar. As expected for a transformed austenite rod, a very different stress-strain response was observed when these results are compared with those of the rods in the as-received martensitic state. Two important differentiating features are the plateau occurring approximately 3-5% strain and the immediately ensuing rapid work hardening response. Similar results are reported in [5]. Furthermore, the hysteresis loops in Test 30 differ from that in Test 21 in Figure 3.5b. For example, each hysteresis loop in Figure 3.6b crosses to the left of the original unloading stress point, i.e. at a lower strain value, whereas the hysteresis loop shown in Figure 3.5b crosses below the original unloading stress point, i.e. at a lower stress value. The observed crossing to the left of the original unloading point in the hysteresis loops suggests a degree of strain recovery occurred during the unload/reload segment in this experiment. A likely explanation for the unload/reload strain recovery and the stress-strain curve plateau observed in the overall stress-strain response of the austenitic samples is that during these experiments, martensite is *stress-induced* from austenite. That is, the stress-induced *austenite-to-martensite* transformation takes place allowing for partial superelastic behavior. In addition to the stress-induced austenite-to-martensite transformation, plastic deformation of the Nb-rich phase and martensite detwinning might have occurred [4, 6, 13].

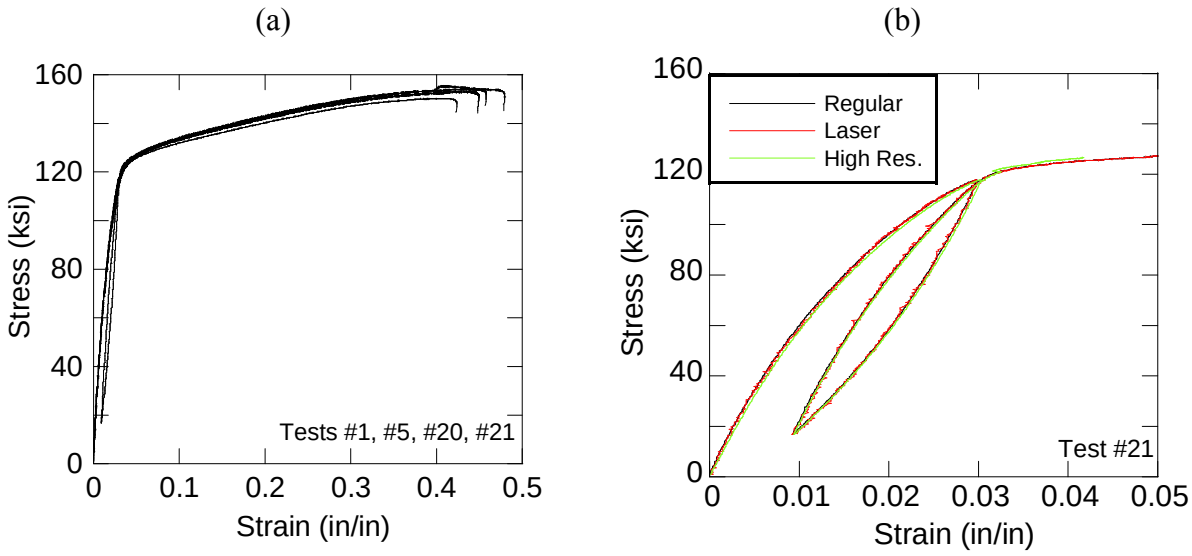

Figure 3.5: RT tension data of as-received, martensitic tensile rods. (a) Entire curves and (b) unload/reload subset comparing three simultaneous, independent strain measurements.

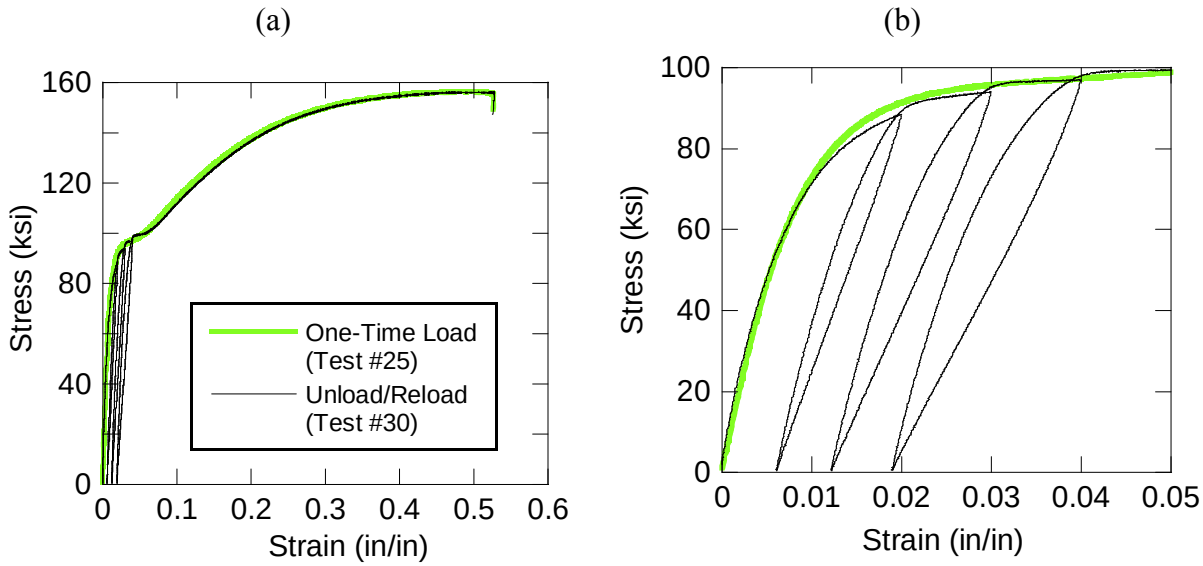

Figure 3.6: RT tension data austenite tensile rods. (a) Entire curves and (b) subset plotted across 0-5% strain range.

Figure 3.7 illustrates a representative comparison of the RT stress-strain response of the martensite (as-received) and austenite rods. The comparison highlights the plateau and work hardening response in the RT austenite results when compared with the RT martensite data. In addition, a 140 °C elevated temperature tensile-test result is compared to the RT data. At 140 °C, the tension rod is almost completely austenitic; however, the temperature is sufficiently high as to suppress the stress-induced transformation to martensite. Thus, the 140 °C tension data offer a better representation of the stress-strain response of austenitic Alloy-H, without the influences of a stress-induced transformations observed in the RT austenite results. Indeed, this seems to be the case since the high temperature tension data show no plateau and a significantly different stress-strain response at strains greater than ~3%.

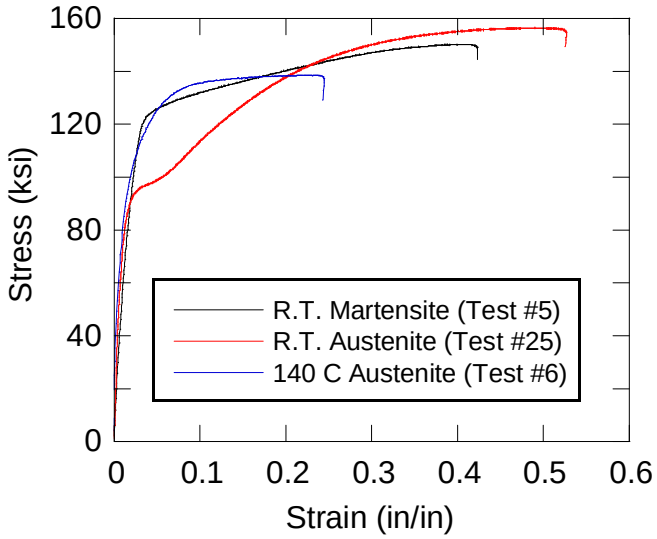

Figure 3.7: Comparison of representative stress-strain curves of Alloy-H in fully martensitic and fully austenitic states.

The second and third series of tension experiments involve straining the tension rods at fixed, elevated temperatures. Figure 3.8 summarizes the stress-strain results for two sets of elevated temperature tension experiments. Figure 3.8a shows results from elevated temperature experiments between RT and 140 °C, where the tensile rods were heated from RT to the listed temperatures at no more than 2 °C/min. Figure 3.8b shows results from experiments performed at temperatures after a half-hour 140 °C excursion. These experiments were performed after cooling from the 140 °C excursion to the listed temperatures. Figure 3.4 illustrates that a majority of the null-load temperature induced martensite-to-austenite transformation occurs at 60 °C. Thus, the mechanical response of Alloy-H between RT and 60 °C was assumed not to change significantly. Correspondingly, elevated temperature tensile test experiments were not performed in this range.

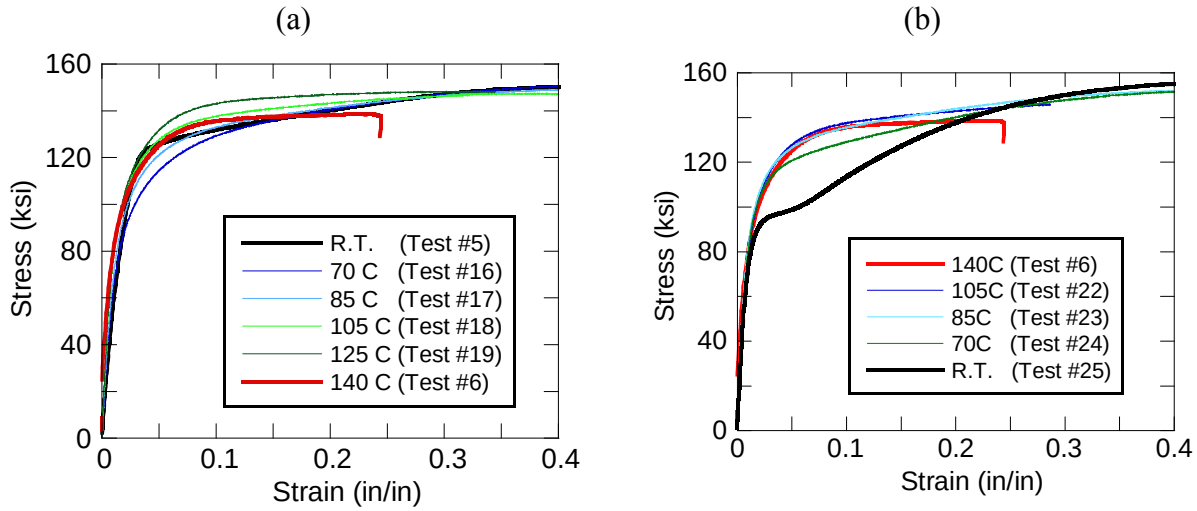

Figure 3.8: Elevated temperature stress-strain curves. (a) Experiments between RT and 140 °C and (b) experiments after a 30 min, 140 °C temperature excursion.

All elevated temperature results in Figure 3.8 show a characteristic sharp bend from a steep slope to a shallow horizontal slope. The characteristic sharp bend occurs at stress and strain values significantly greater than classically defined yield point values determined by the established offset method for tensile test stress-strain curves [7]. Additionally, the results given in Figure 3.8a suggest a trend of decreasing slope with increasing test temperature after the characteristic sharp bend in the stress-strain curves. Although null-load experiments indicate that a majority of the martensite-to-austenite transformation occurs at 60°C, they also indicate the phase transformation continues until the temperature exceeds approximately 130°C. Thus, the decreasing hardening slope shown in Figure 3.8a may correlate with a decrease in residual martensite in the samples. As opposed to the results given in Figure 3.8a, results in Figure 3.8b are those of fully transformed austenite. The 140 °C, 105 °C and 85 °C have shallow hardening slopes, thereby supporting the assumption that the austenitic phase is responsible for this behavior. Furthermore, between ~5% and 15% strain, the 70 °C experiment shows a slight plateau in the stress-strain curve and the RT experiment shows a significant plateau. The stress-induced austenite-to-martensite transformation is most likely responsible and decreasing temperatures are expected to correlate with an increasing ability of the SMA to exhibit the stress-induced transformation [19].

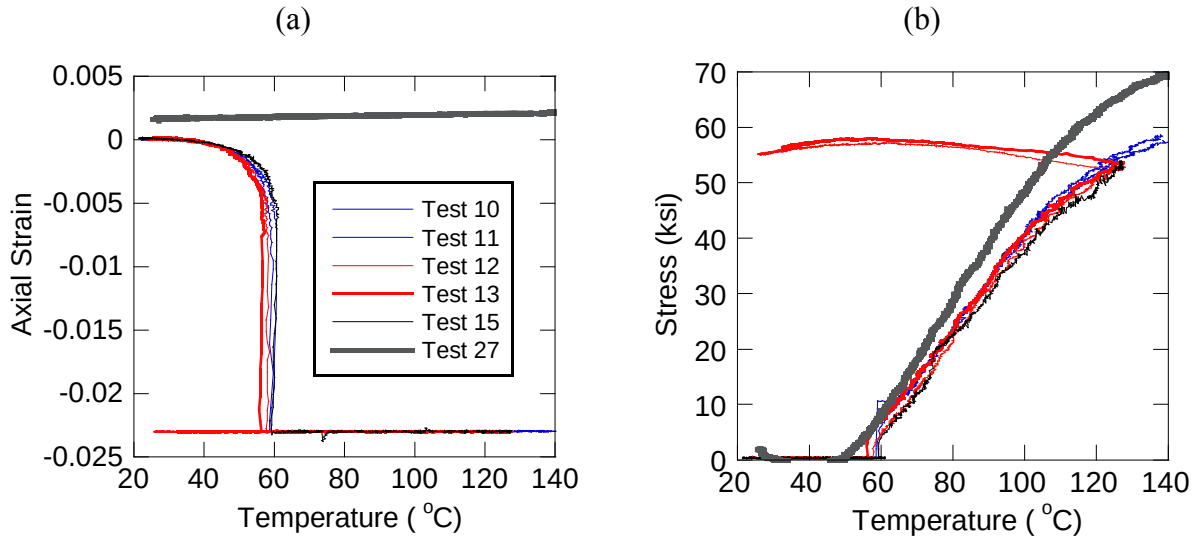

Figure 3.9: (a) Strain vs. Temperature and (b) Stress vs. Temperature results from a series of elevated temperature controlled strain tests.

3.3 Temperature-Controlled Strain and Stress Experiments

Referring to the SMA-based safing wheel design illustrated in Figures 1.3 and 1.4, the design calls for the inner diameter of the SMA rings to be 2.3% larger than the diameter of the ferrite core prior to the core capture step. Therefore, during the assembly process, the SMA ring contracts radially 2.3% before it engages the ferrite core. Once engaged, the core constrains the ring and prevents it from further contraction, resulting in stress generation within the ring. The experimental method and results summarized in this section permit an estimate of the temperature dependent stress within the ring imparted by the constraint of the ferrite core during and after processing. Similar experiments on different test geometries are reported in [1].

To simulate the constrained clamping action within the controlled environment of the thermal chamber, a load of no more than 5 lbf (0.4 ksi) is applied initially to a tension rod at RT. Then, the rod is heated at 2 °C/min, while maintaining the small tensile load and monitoring strain across a 1-2 inch gage section. When 2.3% contraction is detected by the controlling extensometer, the experimental method shifts from load control to strain control and the gage section portion of the tensile rod is held at this strain (henceforth referred to as -2.3% strain). The load required to maintain the -2.3% strain is monitored while the specimen continues to be heated at 2 °C/min. Several experiments were conducted to either 130 °C or 140 °C using this method and the specimen response was also monitored on cool down for at least two of the experiments. The strain vs. temperature results are plotted in Figure 3.9a and stress vs. temperature results, derived from load vs. temperature data, are plotted in Figure 3.9b. Tests 10 and 11 were carried out to 140 °C while Tests 12 and 13 were carried out to 130 °C. Test 15 was controlled across a two inch gage length with the laser extensometer, while the others were controlled across a one inch gage length with the standard extensometer. As shown in Figure 3.9a, all experiments were held after a 2.3% contraction except Test 27 which was held at 0% strain throughout the experiment. The 0% strain result provided a baseline from which the -2.3% strain results could be compared. Stress plotted in this case is nominally the *engineering stress*, where the stress value is defined using the original cross-sectional area of the tension rod.

Results of the five -2.3% strain experiments were consistent. The two experiments conducted to 140 °C showed the restraining stress reached a peak of 57 ksi at this temperature. For comparison, the restraining stress from the 0% strain test reached 67 ksi at 140 °C. Tests 12 and 13, in which stress was monitored during cooling also gave consistent results, showing a slight load increase followed by slight load relaxation presumably due to competing constraint and coefficient of thermal expansion considerations. A change in gage section size proved not to influence the resultant stress vs. temperature curve as evidenced from Test 15, which was controlled by the laser extensometer.

Similar to the strain controlled measurement, stress-strain-temperature space can be investigated in a SMA with stress-controlled experiments as is done in [6]. Two experiments were performed; one where the stress was held at 14.5 ksi (100 MPa) and another where the stress was held at 29 ksi (200 MPa) while the specimen temperature was heated to near 140 °C and cooled to RT. Stress vs. temperature and strain vs. temperature results are given and compared against Test 4 in Figure 3.10. Figure 3.10a confirms that the stress was held constant at the specified value throughout each of the experiments. Figure 3.10b shows that an increase in applied stress delays the onset of the transformation from martensite to austenite along the temperature axis. In addition, the amount of total contraction provided by the transformation decreases with an increase in stress applied to the tensile rods. The reduction in transformation strain at increasing loads is partially due to the increased plastic deformation of Nb-rich phase in the tension rods [6]. It is suspected that further cooling to subambient temperatures in Tests 35 and 36 would result in reverse transformations to detwinned martensite accompanied by partial tensile deformation due to the persisting load.

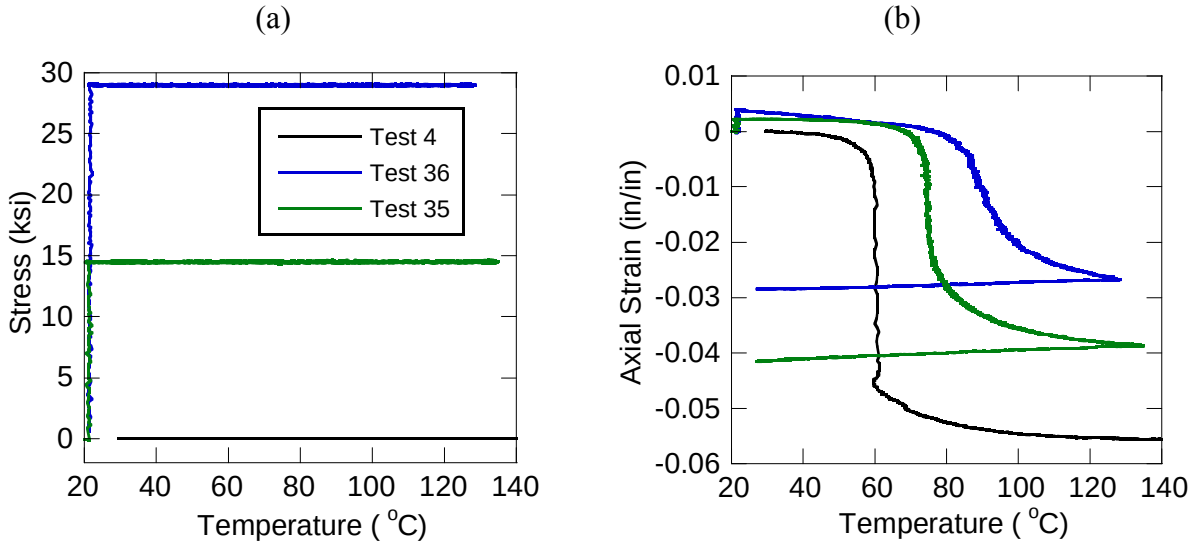

Figure 3.10: (a) Stress vs. Temperature and (b) Strain vs. Temperature constant stress test results. Tests 4, 35, and 36 were performed at 0 ksi, 14.5 ksi and 29 ksi, respectively.

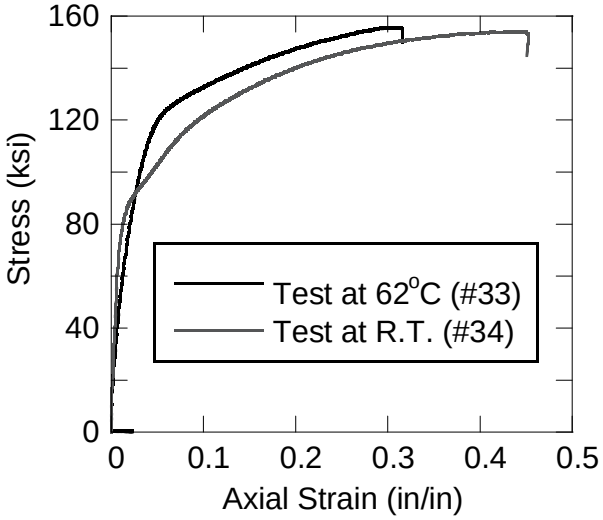

Figure 3.11: Tensile test results on two samples heated and restrained at 2.3% contraction. Test 34 uses the tensile rod contracted during Test 12.

3.4 Tension Test of Partially Transformed Samples

As indicated in Section 3.3, the application of load can suppress the temperature-induced transformation from martensite to austenite. In the clamping ring application, internal stresses develop when the heated ring contacts the ferrite core. Therefore, to complete the mechanical test portion of the SMA study deemed necessary for model validation, tension tests were conducted on two samples allowed to contract 2.3% strain via the temperature induced martensite-to-austenite transformation. Supporting evidence of the stress-induced martensite-to-austenite transformation and resultant plateau in the stress-strain response was sought. The stress-strain results for these two tests are given in Figure 3.11. Test 33 was conducted at 62°C, near the temperature where a majority of the stress-free martensite-to-austenite transformation takes place. Test 34 was conducted at RT and used the tensile rod already transformed and held at -2.3% strain as part of Test 12.

The tensile-test portion of Test 33 begins at 8 ksi, which is the stress required to hold the specimen to -2.3% strain at 62 °C. The resultant stress-strain curve from this test exhibits a sharp bend and a post-bend work hardening rate similar to previously presented results where the sample was known to be in the martensitic state prior to testing, e.g. the RT results given in Figure 3.5. Thus, although the sample is partially transformed and must be constrained to maintain -2.3% strain at 62 °C, martensite still exists within the sample and influences the work hardening during the tensile test portion of the experiment. In addition, apparently the temperature-stress combination suppressed the stress-induced transformation represented by a plateau in the stress strain curve. Test 34 does show a plateau similar to but not as dramatic as that from Test 25. In Test 25, the specimen experienced the stress-free martensite-to-austenite transformation via an elevated temperature excursion prior to testing. In Test 34, the specimen experienced the same transformation under the requisite stress required to maintain -2.3% strain through the temperature excursion. The martensite-to-austenite transformation was hindered and may not have completed, as can be inferred from the results presented in Section 3.3. Nonetheless, some material in the specimen did undergo the transformation to austenite. A portion of the material within the sample was in the austenitic state and therefore was assumed to undergo the stress-induced *austenite-to-martensite* transformation already tied to stress-strain curve plateaus observed in Figures 3.6-3.8 for specimens transformed to austenite. Therefore, Test 34 did offer supporting evidence tying the stress-induced austenite-to-martensite transformation to plateau in the stress-strain curve.

This Page intentionally left blank

4. Parameter Identification

The experiments described in the previous sections were performed with the intent of developing an understanding of the coupled thermo-mechanical behavior of the NiTiNb SMA rings. This section discusses processing of the experimental data to identify parameters for development of a simple constitutive model to be used in simulations of the safing wheel assembly described in Section 1.2. A finite element (FE) implementation of the model is introduced in [15]. The main model parameters used for the NiTiNb SMA ring material are taken from orthotropic thermal strain curves given in Section 2 and the temperature-dependent elastic modulus and plateau stress extracted from the experiments presented in Section 3.

4.1 Thermally-Induced Strain

In the constitutive model, the thermal strain curves indicate how the material expands or contracts in response to temperature in orthogonal material directions. As opposed to requiring temperature-dependent thermal expansion coefficients, which is appropriate for a linear strain-temperature response, the nonlinear temperature-strain response must be completely captured in the constitutive model. Therefore, the data from Figures 2.1 and 2.2 are used to define radial and axial thermally induced strain in the model.

4.2 Modulus and Plateau Stress

The elastic modulus is a classical material property defining the recoverable extension experienced by a material under load. Many materials, such as ceramics, glasses, and most metal alloys, exhibit a well-defined linear elastic regime. In these cases, a fairly accurate measure of a linear elastic modulus can be obtained from tension test data [7]. However, for materials such as soft metals and many polymeric materials, either the elastic response is nonlinear or the material exhibits non-recoverable strain at such low stress values that a linear elastic modulus becomes difficult to accurately measure from tensile test results. The stress-strain curves in Figures 3.5 and 3.6 show that the NiTiNb Alloy-H seems to exhibit both a nonlinear elastic response and a very low stress-threshold for the onset of permanent deformation. The unload-reload hysteresis shown in these figures is very revealing in that regard.

In cases where a linear elastic region is not apparent in the tensile stress-strain response of a material, a *tangent method*, illustrated in Figure 4.1a, may be used to isolate a linear elastic modulus value for the material [7]. The method used fits a cubic curve to the data up to 0.5% strain and subsequently calculates the tangent to the curve at the origin. Ultimately, however, the resultant modulus value may not be useful for capturing the material response in a simple constitutive model, as observed in the figure. In particular, the elastic-plastic constitutive model introduced in [15] assumes that the SMA extends bilinearly, where the material extends with a fixed slope up to a certain point where the slope decreases. The initial slope corresponds to the elastic modulus and the point of intersection represents a *plateau stress* and strain, which for SMAs, represents either a transformation point or a yield point [4, 8, 10, 19].

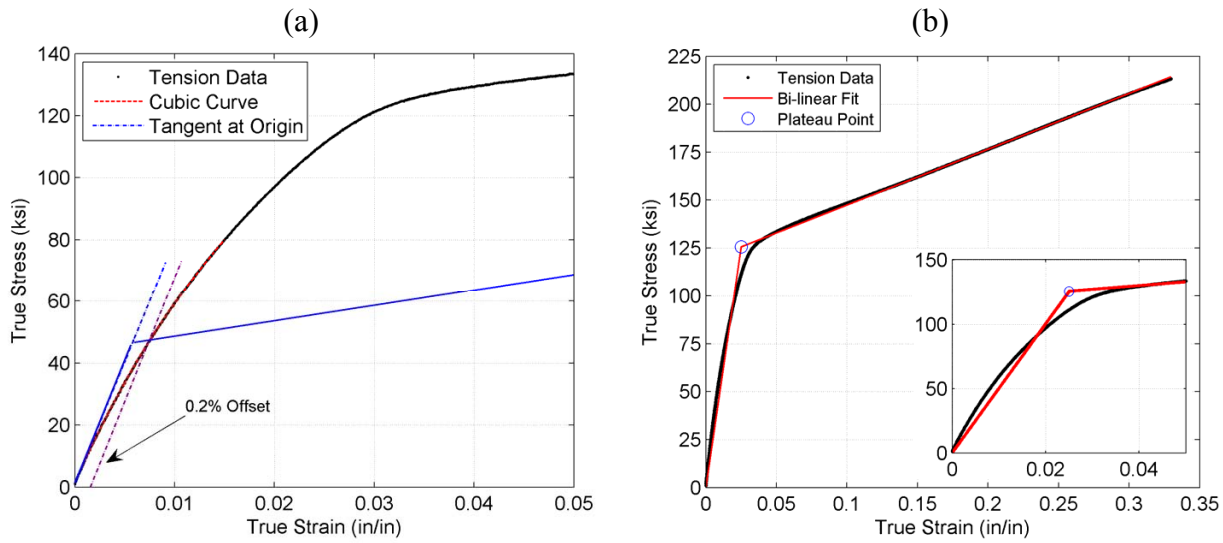

Figure 4.1: Methods for determining elastic and plateau stress: (a) tangent method where the solid blue line represents a constitutive model prediction and (b) secant method via bi-linear fit that represents model prediction.

The general shape of the tensile stress-strain data given in Section 3 suggests that a bilinear fit to the experimental data can capture the response of the NiTiNb SMA, albeit with an alternative interpretation of the fit portion associated with the modulus. Thus, the secant method was used to compute the *secant modulus*, which is the ratio of stress to strain that represents the slope of a line drawn from the origin to a point on the stress-strain curve. The point is referred to as a *plateau* point and it defines the transition from a steep to shallow slope in the tensile stress-strain response of the material. Although the Alloy-H tested does not behave in a linear elastic fashion in the secant modulus regime, it does seem to recover most of its strain upon unloading and the response is approximately linear when considered across the wide range encompassing the entire stress-strain response. Thus, for the purposes of simulating the SMA ring, which does not undergo significant stress-strain cycling during the clamping of the safing wheel assembly, this secant method was deemed a reasonable representation of the mechanical response of the NiTiNb SMA.

Table 4.1: Some moduli calculated using the secant (bi-linear model) and tangent (0.5% strain) methods.

Temperature (°C)	Secant Modulus (ksi)	Tangent Modulus (ksi)
140	7419.7	10244
105	6684.6	9971.3
85	7753.5	15576
70	7737.6	12252
25	8266.6	10095

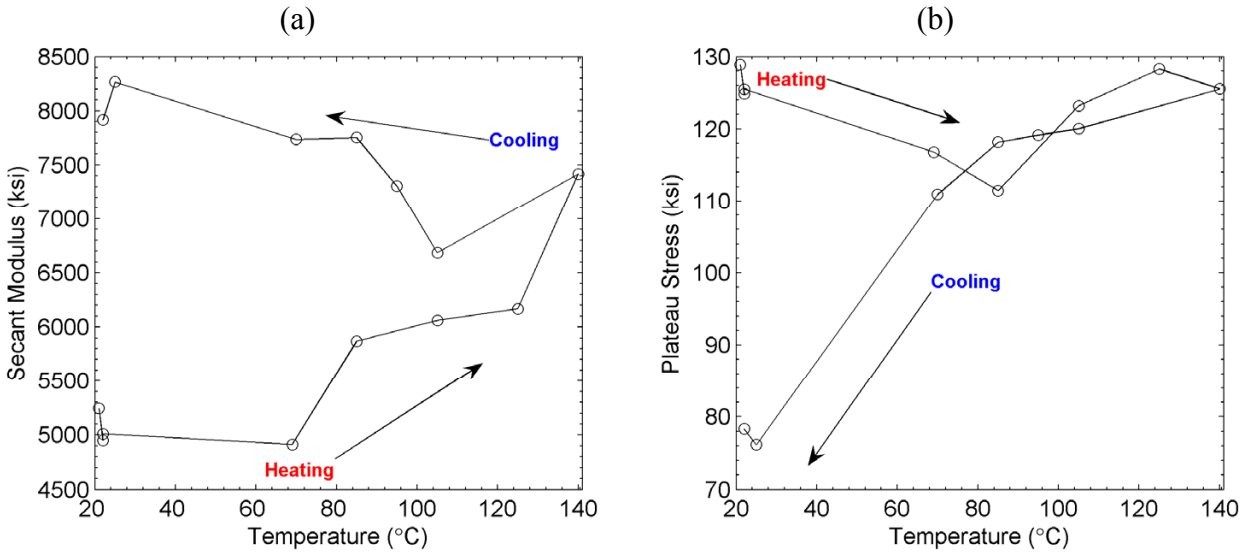

Figure 4.2: Temperature-dependent parameters from bi-linear fits: (a) elastic modulus and (b) plateau stress.

Specifically, the plateau point is determined via a fit of a bi-linear function to the true stress-strain data. The bi-linear function consists of two intersecting linear segments. As illustrated in Figure 4.1a, the tangent method leads to a poor prediction of the stress-strain response for strains greater than 0.5%. As illustrated in Figure 4.1b, the bi-linear fit provides a better, overall representation of the stress-strain response compared to the tangent method. For comparison, Table 4.1 lists the modulus values calculated from both the tangent and secant methods for temperatures cooling from 140 °C. In general, the tangent method produces larger moduli than does the secant method. The modulus and plateau stress computed from the tension data as a function of temperature are plotted in Figure 4.2. Note the hysteresis, which is a result of the interaction of martensite, austenite, and the matrix of Nb particles during the heating and subsequent cooling. The constitutive model used in the FE analysis of the clamping ring behavior can use the data in Figure 4.2 for prescribed temperature-dependent moduli and plateau stresses.

Table 4.2: Calculated moduli and plateau stresses (bi-linear model) for free and clamped tension experiments.

Free/Clamped	Temperature (°C)	Secant Modulus (ksi)	Plateau Stress (ksi)
Clamped	62 (Heat)	3195.1	115.1
Free	69 (Heat)	4913.2	116.8
Free	22 (Cool)	7917.0	78.36
Clamped	21 (Cool)	7765.0	70.05

The data calculated and plotted in Figure 4.2 represents the response under no external loading or constraint. That is, this data was determined from the stress-strain results given in Section 3.2. In the clamping ring application, reaction stresses on the SMA ring during its clamping action on the ferrite core may affect the phase transformation and, in turn, the mechanical response of the SMA. As described in Section 3.4, follow-up tension experiments were performed on two samples that were constrained at -2.3% strain. Secant modulus and plateau stress data from these experiments were determined and given in Table 4.2 with results from comparable tests on unconstrained rods. The difference in secant moduli is slightly larger than the difference in plateau stresses. It is suspected that free and clamped tensile behavior is identical at temperatures cooling from a soak at 140 °C, since this temperature may be sufficiently high to induce a nearly full transformation to austenite, even under the restraint stress. Further study is needed to quantify the effect of restraining the SMA during heating.

Note that the phenomenon responsible for the plateau stress calculated and plotted in Figure 4.2 is yet to be addressed. It is postulated that the plateau stresses above 110 ksi represent the yield stress of the material. As described in Section 3.3, stress-induced transformations from austenite to martensite were observed in only the RT austenite samples. In the next section, an investigation of transformation stress is discussed.

4.3 Transformation Stress

As described in Section 1.1, temperature-dependent, stress-induced transformations can occur in SMAs from austenite to martensite. The loads at which the transformations occur typically increase with temperature. Furthermore, at sufficiently high temperatures, the stress-required to induce the austenite-to-martensite transformation is superseded by the onset of yielding of the austenite phase [9, 19]. Thus, there is a limiting temperature at which the stress-induced austenite-to-martensite transformation is no longer observed, typically denoted M_d. Drawing from the results in Section 3, only the experiments of austenite rods at RT exhibited a plateau stress that was suggestive of the stress-induced transformation. Therefore, M_d of the as-received rods may not be much greater than the temperature where austenite begins to form. Further discussion on the limited temperature range of the stress-induced austenite to martensite transformation in NiTiNb is given in [19], where it is sourced to Nb particles in the material.

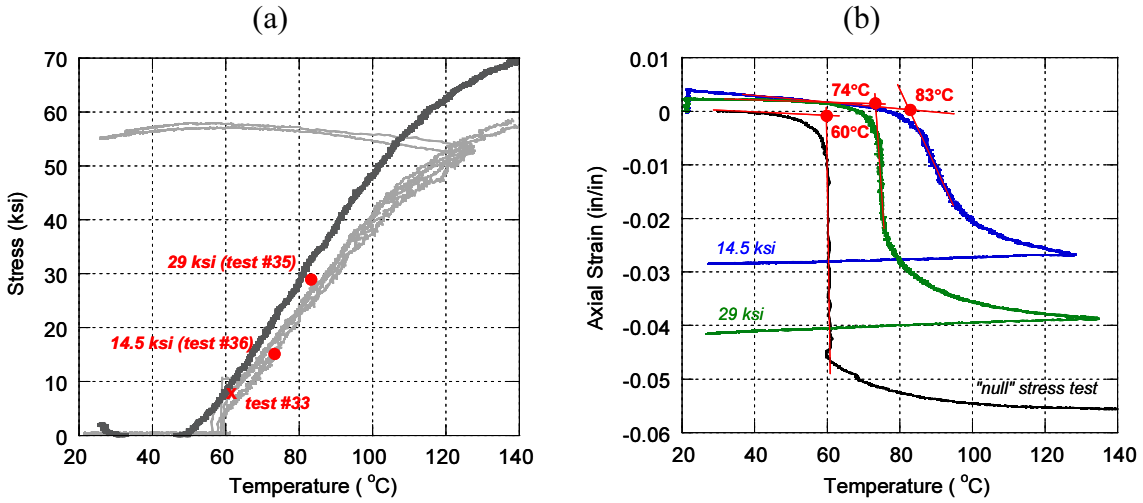

Figure 4.3: Transformation stresses and temperatures: (a) temperature-controlled clamping stress represents temperature-dependent transformation stresses and (b) load-controlled thermal strain providing stress-dependent transformation temperatures.

With regard to incorporating constitutive response into an FE analysis to simulate the safing wheel assembly process, this report is more directly concerned with the effect of stress on delaying the martensite-to-austenite transformation. Results presented in Figure 3.10 can be used to quantify the delaying effect of stress generated in the SMA ring as it clamps the ferrite core on the martensite-to-austenite transformation. For the purpose of capturing this constitutive response in an FE model, it is postulated that the clamping stress supported by the shrinking ring at a given temperature represents the transformation stress at that temperature. In turn, the transformation stress corresponds to the plateau stress before the yield stress is reached. Figure 4.3 illustrates this concept by correlating stress and temperature for the martensite to austenite transformation. The transformation temperature extracted from the strain-temperature curves from the constant stress experiments is estimated using intersecting tangent lines in Figure 4.3b [9]. The resulting stress-dependent transformation temperature can be plotted against the results in Figure 4.3a, allowing for a stress-temperature correlation estimate for the martensite to austenite transformation. Each stress value represented in Figure 4.3a is assumed to be the maximum stress the SMA can exert due to the temperature-induced transformation to austenite. The stress values are also assumed to correlate to a plateau stress as the SMA undergoes a stress-induced transformation to martensite. The exact nature of that correlation is unclear without further experimentation.

Considering the transformation temperature as a function of stress, a linear dependence of approximately 0.9 °C/ksi is calculated from the experiments in Figure 4.3b, where transformation at zero load occurs near 60 °C. Likewise, considering the transformation stress as a function of temperature, the 0% contraction test (Test 27) shows a stress-temperature dependence of approximately 1.0 ksi/°C across the 60-90°C temperature range. Allowing the rods to contract 2.3% before constraining slightly reduces the rate to 0.8 ksi/°C. Ultimately, the data plotted in Figure 4.3a may be treated as plateau stress data used in the constitutive model of the SMA ring in the safing wheel assembly, however, further fixed load experiments should be conducted to confirm this hypothesis and refine the stress-temperature dependence of the martensite-to-austenite transformation.

This Page intentionally left blank

5. Concluding Remarks

This report summarizes efforts to characterize SMAs used in advanced safety mechanism designs. The safing wheel described utilizes the nonlinear material properties of NiTiNb to forcibly clamp a ferrite core. Ultimately, the use of SMA in the safing wheel design greatly simplifies the assembly process, obviates process-sensitive metallization/solder steps, and makes the assembly very robust to mechanical environments. Model-based analysis of the SMA-based assembly process is critical to the advancement and maturation of the safing wheel design [15]. In turn, the constitutive models used require constitutive properties and validation data in order to make reliable predictions.

The Alloy-H NiTiNb used in the SMA-based design was examined via dilatometry, DSC, and an array of thermomechanical tension experiments. The dilatometry quantified the evolution of temperature induced strain in both the radial and axial directions, while the DSC more clearly revealed the onset of the temperature-induced phase transformation. The thermomechanical tension tests provided insight into the mechanical behavior of Alloy-H under conditions similar to those experienced by the ring as it clamps the ferrite core. Altogether, these results demonstrated that the material has unique, nonlinear behavior that is consistent across various sample geometries and batches of the alloy fabricated by the manufacturer. Finally, key constitutive material properties were determined from the experimental results for use in models of the clamping rings. Future experimental investigations should focus on the evolution of transformation stress and transformation temperature and their intrinsic coupling.

This Page intentionally left blank

6. References

1. V.Ya. Abramov, N.M. Aleksandrova, et al., "Structure and functional properties of heat- and thermomechanically treated Ti-Ni-Nb-based alloys with a wide martensitic hysteresis. I. Ti-Ni-Nb ternary alloys," *Phys. Met. Metallogr.*, **101**(4), pp. 404–414, 2006.

2. W. Cai, C.S. Zhang, L.C. Zhao, "Recovery stress of Ni-Ti-Nb wide-hysteresis shape memory alloy under constant strain and thermomechanical cycling," *J. Mat. Sci. Letters*, Vol. 13, pp. 8-9, 1994.

3. W. Cai, X.L. Lu and L.C. Zhao, "Damping behavior of TiNi-based shape memory alloys," *Mater. Sci. Eng. A, Struct. Mater., Prop. Microstruct. Process.*, **394**(1-2), pp. 78–82, 2005.

4. X.M. He, L.J. Rong, et al., "Study of the $Ni_{41.3}Ti_{38.7}Nb_{20}$ wide transformation hysteresis shape-memory alloy," *Metall Mat Trans A Phys Metall Mat Sci*, **35A**(9), pp. 2783-2788, 2004.

5. X. He, D. Yan, et al., "Effect of Nb-content on mechanical properties of $(Ni_{47}Ti_{44})_{100-x}Nb_x$ shape memory alloys," *Mater. Sci. Forum*, Vol. 475-479, Pt. 3, pp. 1945-1948, 2005.

6. W. Jin, M. Cao, et al., "Effect of restraint stress on transformation temperatures and strain recovery in a $Ni_{47}Ti_{44}Nb_9$ shape-memory alloy," *Mater. Sci. Forum*, Vol. 394-395, pp. 273-276, 2002.

7. H. Kuhn, "Tension, Compression, Bend, and Shear Testing," *ASM Handbook Volume 08: Mechanical Testing and Evaluation*, Eds. H. Kuhn and D. Medlin, ASM International, Materials Park, Ohio, pp. 124-140, 2000.

8. M. Kusagawa, T. Nakamura and Y. Asada, "Fundamental deformation and recovery behaviors of Ni-Ti-Nb shape memory alloy," *JSME Int. J. A, Solid Mech. Mater. Eng. (Japan)*, **44**(1), pp. 57-63, 2001.

9. K. Otsuka and C.M. Wayman, *Shape Memory Materials*, Cambridge University Press, Cambridge, 1999.

10. O. Oyamada, K. Amano, et al., "Effect of environment on static tensile and fatigue properties of Ni-Ti-Nb shape memory alloy," *JSME Int. J. A, Solid Mech. Mater. Eng.*, **42**(2), pp. 243-248, 1999.

11. J. Shaw and S. Kyriakides, "Thermodynamic aspects of NiTi," *J. Mech. Phys. Solids*, **43**(8), pp. 1243-1281, 1995.

12. W. Siegert, K. Neuking, et al., "First cycle shape memory effect in the ternary NiTiNb system," *J. Phys. IV, Colloq. (France)*, **112**(2), pp. 739-742, 2003.

13. Y. Suzuki and H. Horikawa, "Thermal hysteresis in Ni-Ti and Ni-Ti-X alloys and their applications," *Shape-Memory Materials and Phenomena – Fundamental Aspects and Applications*, Vol. 246, pp. 389-398, 1992.

14. T. Takagi, Y. Sutou, et al., "Effect of Prestrain on Martensitic Transformation in a $Ti_{46.4}Ni_{47.6}Nb_{6.0}$ Superelastic Alloy and its Application to Medical Stents," *J. Biomed. Mater. Res. Part B*, **76B**(1), pp. 179-183, 2006.

15. R. Tandon, J.T. McLaughlin, et al., "Component Development using a Coupled Analysis and Experimental Approach: Ceramic-Ceramic and Ceramic-Metal Joining," *Brazing and Soldering: Proc. Third Internat. Brazing and Soldering Conf.*, pp. 67-72, 2006.

16. V.A. Udovenko, P.L. Potapov, et al., "A study of the functional properties of alloy Ti-45% Ni-10% Nb with wide hysteresis of the martensitic transformation," *Met. Sci. Heat Treat.*, **42**(9-10), pp. 353-356, 2000.

17. L. Wang, L.J. Rong, et al., "DSC study of the reverse martensitic transformation behavior in a shape memory alloy pipe-joint," *Intermetallics*, **13**(3-4), pp. 403-7, 2005.

18. L. Wang, D.S. Yan, et al., "Shape memory alloy pipe-joint with copper coating," *Materials Science Forum*, Vol. 475-479, pt. 3, pp. 1957-1960, 2005.

19. J.H. Yang and J.W. Simpson, "Stress-induced transformation and superelasticity in Ni-Ti-Nb alloys," *J. Phys. IV, Colloq. (France)*, **5**(C8), pt. 2, pp. 771-776, 1995.

20. Y.F. Zheng, W. Cai, et al., "Effects of heat treatment on the transformation temperature and the microstructure of Ni-Ti-Nb shape memory alloy," *J Mater Sci Technol*, **14**(1), pp. 37-40, 1998.

Appendix A: NiTiNb Alloy-H Experiment Log

Table 6.1: Log of experiments. All soak periods are 30 minutes unless otherwise noted.

Test No.	Sample No.	Date	File Name	Characterization Type	Experiment Description	Batch
1	1	6/29/2005	062905_sma_1e-3_rt	Modulus (Heating)	RT (22C) Tension Test, 10^{-3}/s	
2	2	7/11/2005	071105_sma_2e-3_130c	Modulus (Heating)	ramp to 140C, 6 C/min, tension test, 2e-3/s	
3	3	8/4/2005	080405_sma_constdisp_reduced	Clamping Load Capacity	constant crosshead disp., 40-135C, 6.5 C/min, cool to RT	
4	4	8/12/2005	081205_sma_constload_reduced	Thermal Strain	ramp to 141C, 3.8 C/min, constant load, 5 lbf	
5	5	9/29/2005	092905_sma test #5_mod	Modulus (Heating)	RT (22C) Tension Test, 4e-4/s	
6	6	9/29/2005	092905_sma_hitemp_test#6_mod_p2	Modulus (Heating)	ramp to 140C, 2 C/min, tension test, 4e-4/s	
7	7	9/29/2005	sma_092905_test#7_mod	Clamping Load Capacity	hold at -2.3% strain, ramp to 140C, 2 C/min, first attempt, bad feedback control	
8	8	10/19/2005	sma_101905_test#8.dat	Clamping Load Capacity	hold at -2.3% strain, ramp to 130C, 2 C/min, second attempt, mis-programmed control	Batch 1
9	9	10/19/2005	sma_101905_test#9_mod	Clamping Load Capacity	hold at -2.3% strain, ramp to 140C, 2 C/min, third attempt, bad test	
10	10	11/12/2005	sma_112105_test#10	Clamping Load Capacity	hold at -2.3% strain, ramp to 140C, 2 C/min	
11	11	11/22/2005	sma_112205_test#11	Clamping Load Capacity	hold at -2.3% strain, ramp to 140C, 2 C/min	
12	12	2/7/2006	sma_020706_test#12_mod	Clamping Load Capacity	hold at -2.3% strain, ramp to 130C, 2 C/min, cool to RT	
13	13	2/7/2006	sma_020706_test#13_mod	Clamping Load Capacity	hold at -2.3% strain, ramp to 130C, 2 C/min, cool to RT	
14	14	2/15/2006	sma_021506_test#14_mod	Clamping Load Capacity	hold at -2.3%strain, extensometer slipped	
15	15	2/16/2006	sma_021606_test#15_mod	Clamping Load Capacity	hold at -2.3%strain, laser controlled (2 in gauge), cool to RT	
16	16	2/21/2006	sma_022106_test#16_mod, sma_022106_test#16b_mod	Modulus (Heating)	ramp to 69C, 2 C/min, tension test, 10^{-4}/s; automatic temperature trigger failed.	
17	17	2/23/2006	sma_022306_test#17_mod	Modulus (Heating)	ramp to 85C, 2 C/min, tension test, 10^{-4}/s	
18	18	2/23/2006	sma_022306_test#18_mod	Modulus (Heating)	ramp to 105C, 2 C/min, tension test, 10^{-4}/s	
19	19	2/24/2006	sma_022406_test#19_mod	Modulus (Heating)	ramp to 125C, 2 C/min, tension test, 10^{-4}/s	
20	20	3/24/2006	sma_032406_test#20_mod	Modulus (Heating)	RT (22C) Tension Test, 10^{-4}/s, hi-res extens.	
21	21	3/27/2006	sma_032706_test#21_mod	Modulus (Heating)	RT (21C) Tension Test, 10^{-4}/s, load to 3%, unload to 200 lbf, reload to failure, hi-res. extens; failed at head	
22	22	3/27/2006	sma_032706_test#22_mod	Modulus (Cooling)	ramp to 140C, soak, cool to 105C, soak, tension test, 10^{-4}/s; failed at head	
23	23	3/28/2006	sma_032806_test#23_mod	Modulus (Cooling)	ramp to 140C, soak, cool to 85C, soak, tension test, 10^{-4}/s; failed at head	
24	24	3/28/2006	sma_032806_test#24_mod	Modulus (Cooling)	ramp to 140C, soak, cool to 70C, soak, tension test, 10^{-4}/s	
25	25	3/30/2006	sma_033006_test#25_mod	Modulus (Cooling)	ramp to 140C, soak, cool to RT (25C), soak, tension test, 10^{-4}/s	Batch 2
26	26	3/30/2006	sma_033006_test#26.dat	Clamping Load Capacity	hold at 0% strain; failed test.	
27	27	3/30/2006	sma_033006_test#27_mod	Clamping Load Capacity	hold at 0% strain, ramp to 140C, 4 C/min	
28	28	4/28/2006	sma_042806_test#28_mod	Modulus (Cooling)	ramp to 140C, soak, cool to 95C, soak, load to 3%, unload to 100 lbf, reload to failure, 10^{-4}/s	
29	26	5/17/2006	sma_051706_test#29_mod.txt	Clamped Modulus (Cooling)	RT (20C) Tension Test, 10^{-3}/s, load to 2%, unload to 5 lbf, repeat for 3%, 4%, reload to failure, test setup for Test	
30	4	5/18/2006	sma_051806_test#30_mod.txt	Modulus (Cooling)	RT (22C) Tension Test, 10^{-4}/s, load to 2%, unload to 5 lbf, repeat for 3%, 4%, reload to failure; collet slipped near	
31	-			Test Setup		
32	-			Test Setup		
33	29	5/18/2006	sma_051806_test#33_mod.txt	Clamped Modulus (Heating)	hold at -2.3% strain, ramp to 62C, 1 C/min, soak, tension test, 10^{-4}/s	
34	12	6/13/2006	sma_061306_test#34_mod.txt	Clamped Modulus (Cooling)	RT (21C) Tension Test, 10^{-4}/s, load to failure.	
35	30	6/14/2006	sma_061406_test#35_mod.txt	Fixed Load Thermal Cycle	load to 350 lbf, 5 lbf/s, hold load, heat to 50C, 2 C/min, 50-120C, 1 C/min, 130C, 2 C/min, soak 1 hr, cool to RT.	
36	31	6/21/2006		Fixed Load Thermal Cycle	load to 175 lbf, 5 lbf/s, hold load, heat to 50C, 2 C/min, 50-120C, 1 C/min, 130C, 2 C/min, soak 1 hr, cool to RT.	

DISTRIBUTION:

1	MS0349	Jamey T. Bond	02613
4	MS0349	Kenneth Eras	02613
1	MS0372	Matthew A. Neidigk	01524
1	MS0372	James M. Redmond	01525
1	MS0847	Pavel M. Chaplya	01526
1	MS0886	Donald F. Susan	01813
1	MS0889	Thomas E. Buchheit	01814
1	MS0889	Michael F. Hosking	01813
1	MS0889	Rajan Tandon	01825
1	MS0899	Technical Library	09536 (electronic copy)
1	MS1064	Coby L. Davis	02614
1	MS1064	Rick A. Kellogg	02614
2	MS1070	Jordan E. Massad	01526
1	MS1070	Chungnin C. Wong	01526
1	MS1245	Ronald S. Goeke	02452
1	MS9154	Jared T. McLaughlin	12346
1	MS9404	Jonathan A. Zimmerman	08776


Sandia National Laboratories